A Two-step Surface-based 3D Deep Learning Pipeline for Segmentation of Intracranial Aneurysms

Xi Yang
The University of Tokyo

Ding Xia
The University of Tokyo

Taichi Kin
The University of Tokyo

Takeo Igarashi
The University of Tokyo

arXiv:2006.16161v2 [eess.IV] 4 Jul 2021

ABSTRACT

The exact shape of intracranial aneurysms is critical in medical diagnosis and surgical planning. While voxel-based deep learning frameworks have been proposed for this segmentation task, their performance remains limited. In this study, we offer a two-step surface-based deep learning pipeline that achieves significantly higher performance. Our proposed model takes a surface model of entire principal brain arteries containing aneurysms as input and returns aneurysms surfaces as output. A user first generates a surface model by manually specifying multiple thresholds for time-of-flight magnetic resonance angiography images. The system then samples small surface fragments from the entire brain arteries and classifies the surface fragments according to whether aneurysms are present using a point-based deep learning network (PointNet++). Finally, the system applies surface segmentation (SO-Net) to surface fragments containing aneurysms. We conduct a direct comparison of segmentation performance by counting voxels between the proposed surface-based framework and the existing voxel-based method, in which our framework achieves a much higher dice similarity coefficient score (72%) than the prior approach (46%).

CCS CONCEPTS

• **Applied computing** → **Health informatics**; • **Computing methodologies** → **Computer vision problems**.

KEYWORDS

Intracranial aneurysm segmentation, Point-based 3D deep learning, Medical image segmentation

1 INTRODUCTION

An intracranial aneurysm (IA) is a weakened or thinned portion of a blood vessel in the brain that bulges dangerously and fills up with blood. Bloated aneurysms compress the surrounding nerves and brain tissue and have a high risk of rupture, resulting in subarachnoid hemorrhage (SAH). The risk of such rupture is related to the size and form of the IA [6]. The practical surgical approach is to clip their neck to prevent the rupture. Therefore, extracting the shape of aneurysms is a crucial aspect not only of IA diagnosis but also of preoperative examination to determine the position and posture of the necessary clips [1]. In current practice, this process requires manual identification by medical experts, taking several minutes per case. Clearly, automating this process is a very worthwhile venture. Furthermore, employing automation, we can also obtain large segmented datasets, which can open up new avenues for research toward gaining further insights into IA through statistical analysis.

Table 1: Comparison of related works and our method.

	Entire image (Practicality)	Surface-based (Effectiveness)
Park et al. [17] & Sichterman et al. [21]	✓	✗
Yang et al. [25] & Bizjak et al. [3]	✗	✓
Our	✓	✓

Over the last decade, many extraction algorithms have been designed by calculating local geometric features [12, 16]; however, rule-based methods have high computational costs and time requirements, and their performance is limited because of the wide variety of aneurysm shapes. Meanwhile, deep learning techniques are becoming increasingly popular in medical image processing; however, they are mostly used for classification and detection. Few prior research works have explored the application of deep learning methods to the segmentation of IAs, and their performance remains limited [16] (see Section 2).

This study builds on Yang et al.'s work the IntrA dataset [25], which was created for surface-based classification and segmentation of IAs, and reported the performance of existing neural network models on both tasks. However, in their work, the dataset and execution process were fully separated for both classification and segmentation tasks. Segmentation was evaluated only on manually sampled surface fragments containing aneurysms. This process is unrealistic in clinical practice. In addition, the per-fragment segmentation results were not integrated. Therefore, in this study, we present a complete processing pipeline for segmenting IAs, as shown in Figure 1, by integrating deep learning and geometry processing techniques to achieve better performance. Our proposed pipeline takes an entire intracranial vessel network model as input and returns IA fragments as output.

The main contributions of this study are as follows:

(1) We propose a complete pipeline using point-based 3D deep neural networks for aneurysm segmentation from entire medical images. The proposed pipeline with automatic sampling achieves SOTA results comparable to segmentation based on manual sampling [25].
(2) We demonstrate the advantage of our two-step pipeline combining a classification step and a segmentation step by comparing it against a segmentation-only pipeline.

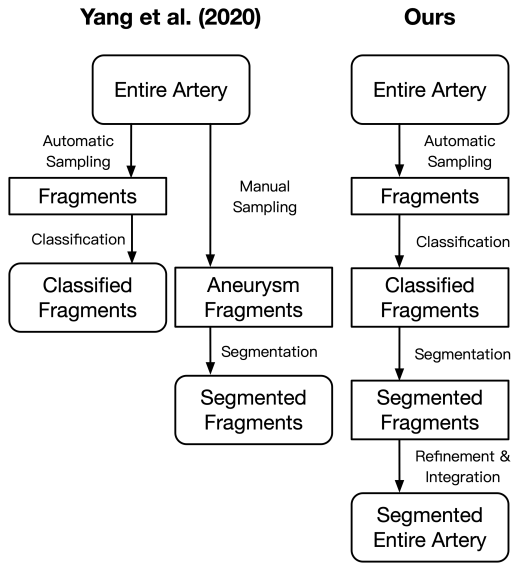


Figure 1: Comparison of the pipeline of Yang et al. [25] and Ours.

(3) We present a direct comparison between our surface-based framework and a SOTA voxel-based method, showing the superiority of our proposed framework.

2 RELATED WORKS

In the field of computer vision in general, detection tasks usually involve determining the rough location and size of target objects, for example, a boundary box, whereas, in medical imaging, detection may indicate only the presence of target objects. The difficulties of both are lower than those of the segmentation task, which requires algorithms to predict the precise shape of the target objects.

2.1 Detection

Deep learning methods have been widely used as diagnosis aid to detect IAs. Nakao et al. [14] detected intracranial aneurysm-based MRA images using a basic deep convolutional neural network. Ueda et al. [23] used ResNet-18 for an automated diagnosis of cerebral aneurysms from TOF MR angiography image data from several sources. In particular, Zhou et al. [26] proposed a transferable multi-model ensemble (MMEN) architecture to predict the possibility of aneurysms using a mesh model. This approach used 3D objects as input, but also still used 2D neural networks by conformal mapping.

2.2 Segmentation

Segmentation of IAs requires obtaining detailed location and shape information of an aneurysm. Conventional approaches have used rule-based 2D or 3D shape analyses. For example, Nikravanshalmani et al. [15, 16] used a level set algorithm and a region growing based approach for the semi-automatic segmentation of cerebral aneurysms from CTA images. Law et al. [11, 12] proposed an intensity-based algorithm to segment intracranial vessels and embedded aneurysms using multirange filters and local variances. Wang et al. [24] presented a multilevel segmentation method based on the lattice Boltzmann method (LBM) and level set with ellipse for accurate segmentation of intracranial aneurysms. Sulayman et al. [22] proposed a scheme for semi-automatic detection and segmentation of intracranial aneurysms. Dakua et al. [4] presented a PCA-based approach to segmenting the brain vasculature in low contrast cerebral blood vessels. Jerman et al. [7] proposed automated cutting plane (ACP) positioning, which is based on the detection of specific geometric descriptors of an aneurysm and its parent vasculature.

Recently, learning-based methods have become increasingly popular alongside the development of deep learning. However, few studies have focused on the segmentation of IAs. Podgorsak et al. [18] claimed that segmenting IAs and the surrounding vasculature from digital subtraction angiography (DSA) images using a convolutional neural network was non-inferior to manually identifying the contours of aneurysms. However, they extracted only 2D contours of the IAs. Park et al. [17] developed a neural network segmentation model called HeadXNet to generate voxel-by-voxel predictions of intracranial aneurysms on tomographic angiography (CTA) imaging to augment the performance of clinical intracranial aneurysm diagnosis. However, they evaluated their model based on the sensitivity, specificity, and accuracy of the entire image; these metrics cannot reflect actual segmentation performance in practice. Sichtermann et al. [21] applied a popular software-based on a volume-based neural network, called DeepMedic [8], to segment IAs from MRA images. However, the performance of their approach was suboptimal (46% in DSC). Importantly, Yang et al. [25] and Bizjak et al. [3] made useful attempts to apply point-based networks to segment IAs. However, segmentation was only performed for surface fragments that were manually labeled as containing aneurysms. This process is unrealistic in clinical practice. In addition, Bizjak et al. [3] employed only the sensitivity of the entire input as an evaluation metric.

2.3 3D deep learning

3D surface models have several representations, including projected view, voxel/pixel, point cloud, and mesh. Voxel-based deep learning approaches are easy to implement using networks developed for 2D image tasks. However, point-based methods have shown great promise and improved performance compared with previous voxel-based methods in the field of 3D shape analysis using deep learning [19]. In addition, using point-based rather than mesh-based methods [5] avoids arduous pre-processing steps, including cleaning the models and constructing manifold meshes. A problem with point-based methods is that they require surface models and cannot be directly applied to medical images. Therefore, we introduce an interactive surface reconstruction process before applying point-based classification and segmentation. We leverage Yang et al. [25]'s surface model data set for training and evaluation.

3 PROPOSED PIPELINE

Figure 2 compares our surface-based pipeline with a voxel-based method. In the voxel-based method [21], the medical image is directly fed to a neural network, which affixes a label to each voxel indicating whether it is part of an aneurysm or not.

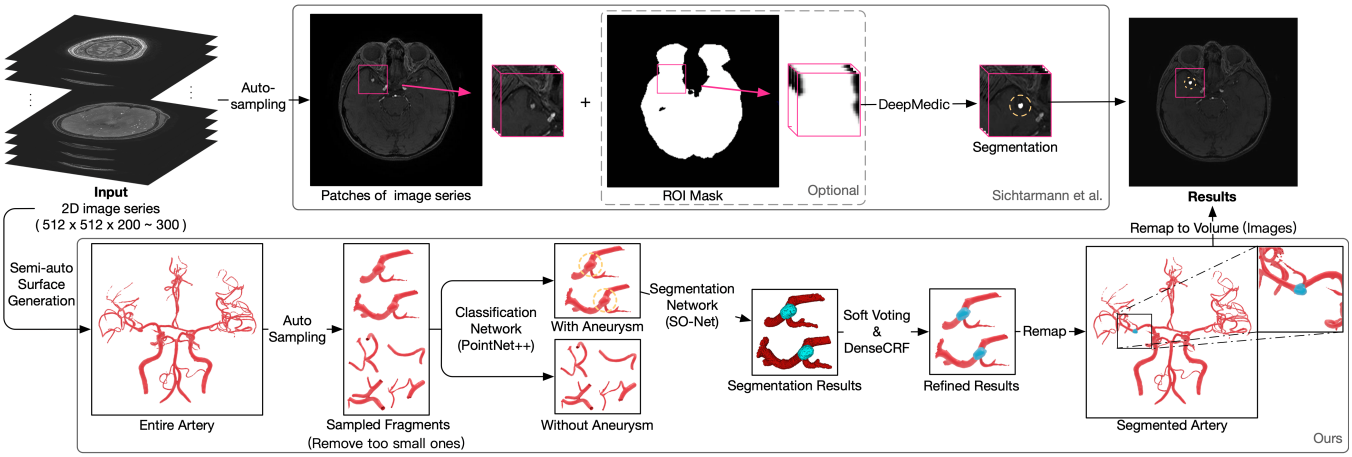


Figure 2: Comparison of our proposed pipeline and voxel-based method.



Figure 3: In contrast to grid sampling, our sampling based on geodesic distance avoids noisy blood vessels are involved.

Our surface-based pipeline first interactively reconstructed a surface model of the entire principal brain arteries using a multiple threshold method. We then generated small samples along vessels within the entire model and performed surface-based classification (PointNet++) on them. Finally, we performed surface-based segmentation (SO-Net) on samples classified as containing aneurysms. To compare our results with the results obtained by voxel-based methods, we voxelized the surface model of the segmented aneurysms into volumes using winding-numbers [2].

3.1 Interactive reconstruction of surface models

We first obtained surface models of the principal brain arteries of patients using TOF-MRA image sets. We performed this semi-automatically using a software package (Amira 2019 by Thermo Fisher Scientific, MA, USA) based on a multi-threshold method [9]. Importantly, we focused on dealing with the brain regions surrounding aneurysms to ensure that the complete shape of the aneurysms was exhibited in the extracted 3D surface model, compared with the data in Intra [25]. In the future, we envision that this process can be mostly or fully automated using a reconstruction network specifically designed for brain arteries.

3.2 Fragments sampling

The segmentation network does not work well if the entire model is input directly because the aneurysm portions are tiny compared to the entire model. Therefore, we first sampled small fragments from the entire model. A typical method used to obtain small patches in medical images involves systematically sampling rectilinear boxes; however, it is difficult to obtain clean artery surfaces because surface boundaries are not aligned with canonical axes. Thus, we designed a sampling algorithm along a surface, as shown in Figure 3. We first set the size of the fragments such that they roughly covered an aneurysm of typical size according to the experience of the medical experts. Then, we divided the 3D space into regular grid cells. From the center of each grid cell, the nearest point on the surface model closer than a threshold (α) was selected as a starting point, while grid cells that did not have nearby surface model points were ignored. Finally, we collected the surface points around the starting points whose geodesic distance was less than a threshold (β). Note that this sampling was designed to cover the model with some overlap; thus, uniform sampling is not a vital requirement of our proposed method.

3.3 Classification step

We used PointNet++ [20] to classify the fragments into two classes, distinguishing those with and without aneurysms. Fragments with few points were discarded before classification. However, the number of fragments with aneurysms was still significantly fewer than those without aneurysms. Therefore, we used a weighted soft-max cross-entropy loss function to train the classification network to deal with the imbalance between the two classes. The purpose of the classification step was to reduce the number of candidate fragments fed to the segmentation network and improve its accuracy.

By design, we sacrifice some classification performance to obtain a better segmentation result. See Section 4.4 for a detailed discussion. The evaluation of our classification results was not fully equal to the accuracy of the detection task. Our sampling method allows one IA to be sampled into several fragments, and fragments with a tiny portion of IA may be misclassified, but the same IA could be detected from other fragments. Therefore, the real-world detection performance results are much better than the performance of the classifier itself.

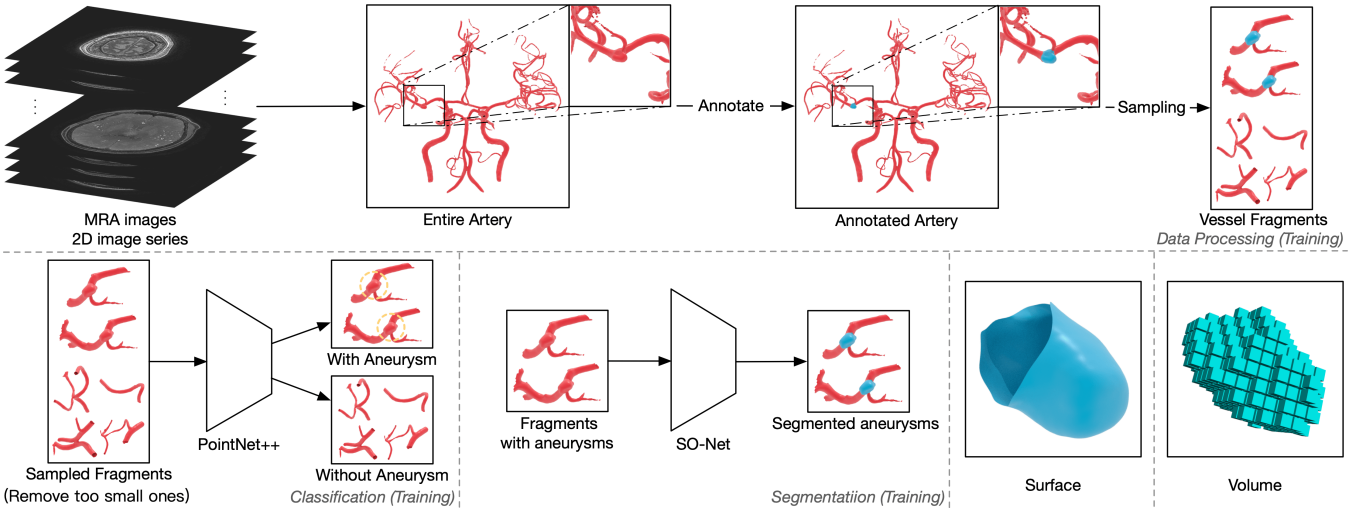


Figure 4: Details of our data-processing pipeline and algorithm.

We expected the classification step to reduce training and prediction time as well as data noise in the final segmentation result. To demonstrate this, we conducted an experiment comparing results between the proposed two-step pipeline and a pipeline without the classification step (Section 4.5.2).

3.4 Segmentation step

We then fed fragments with aneurysms into the segmentation network, SO-Net [13]. Only a fraction of the original points were classified after segmentation because the point-based network uses random sampling to deal with input models with varying numbers of points. Thus, we performed segmentation with random sampling multiple times and assigned labels to all the points based on a voting criterion to enrich segmentation details. There was the possibility of a small number of points failing to be sampled; we labeled them arteries rather than aneurysms; however, these were few, and did not significantly affect the segmentation results. Next, we used a conditional random field (CRF) to refine each voting result, specifically DenseCRF [10]. Finally, the segmentation results of the individual fragments were remapped into the original entire model using a global ID for each point to obtain a complete segmentation result over the entire surface. Points in overlapped parts are commonly sampled twice, so we did not use majority voting. Points with multiple labels were marked as aneurysms if they had an aneurysm label.

3.5 Voxelization

We converted the results of our surface-based segmentation to volume to perform a direct comparison with voxel-based methods. An example is shown in Figure 4. We first obtained a set of the query points through uniform sampling using the same interval as the MRA images. We then computed the winding number of each query point using the fast winding number method [2] to determine whether a given point was inside or outside an aneurysm. We set the threshold of the winding number to 0.5, as suggested in their study. This step is not necessary for clinical practice if segmentation results are required only on the surface model.

4 EXPERIMENTS

Various medical imaging techniques, such as computed tomography angiography (CTA), magnetic resonance angiography (MRA), and digital subtraction angiography (DSA) can be used to obtain images of the brain. DSA is the most sensitive method for diagnosing intracranial IAs; however, it is invasive and time-consuming. Although CTA scans are efficient, distinguishing the details of vessels and aneurysms using CTA remains difficult. TOF-MRA is a less invasive examination and has a high sensitivity for diagnosing IAs. Therefore, we decided upon TOF-MRA as a suitable technique for preoperative examination. However, our proposed pipeline is not affected by the type of medical image, as it is based on reconstructed surface models.

4.1 Dataset

We collected TOF-MRA image sets of 103 patients with 114 aneurysms. Each set contains at least one IA, and $512 \times 512 \sim 300$ 2D images sliced by $0.496mm$. Our dataset does not include small aneurysms (<3.00 mm), because our objective is to segment the aneurysms requiring surgery. We calculated the size of each aneurysm based on maximum diameter, and Figure 5 shows the distribution (Mean: 7.49 mm, SD: 2.72 mm; Range: 3.48–18.66 mm) of aneurysm sizes on our dataset. In terms of IA type, most of our data were saccular aneurysms, and one fusiform aneurysm was included, but no dissecting aneurysm. Another special case was that we treated two aneurysms very close together as being one. We annotated the aneurysm portions on both the entire surface models of the brain arteries and on TOF-MRA images to generate a ground truth for classification and segmentation for training neural networks. It took a total of three experts 21 working days to perform this task. We used five-fold cross-validation to conduct our experiments. A total of 103 sets were shuffled and divided into five subsets, of

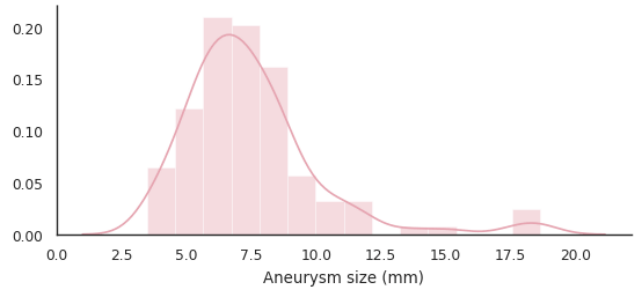


Figure 5: Distribution of aneurysm sizes on our dataset. Mean: 7.49 mm, SD: 2.72 mm; Range: 3.48–18.66 mm.

which four were used as the training data, and one was used as testing data. This study design was approved by an appropriate ethics review board.

4.2 Evaluation metrics

Several evaluation metrics were employed to demonstrate the performance of the models according to different tasks. Accuracy, recall, and sensitivity are typically used to evaluate performance on classification tasks. For the segmentation task, the Dice similarity coefficient (DSC) or Intersection over Union (IoU) is employed to indicate the prediction of the target region. The sensitivity of the entire input can be easily high because the target region may be tiny. Moreover, in this situation, the overall statistics may conflict with the part-wise statistics due to Simpson's paradox.

4.3 Implementation details

The experiments were performed on a PC with a GeForce RTX 2080Ti. During data preprocessing, the normal vector of each point was estimated using the original surface model. We also recorded the point index of the entire model as a global ID on the sampled fragments for each point to improve the efficiency of voting. We set the sampling thresholds as $\alpha = 15, \beta = 1.5 * \alpha$, and the samplings in which the number of points was less than 500 were removed. We automatically generated 7192 vessel fragments from the 103 entire models, and 392 fragments contained aneurysms.

The training hyper-parameters were set as follows. For the classification network, the number of sampling points for each fragment was 1024. The weights of the loss function were determined according to the number of fragments. We trained the network using 251 epochs and a batch size of 8. The classification results were predicted by setting a discrimination threshold of 0.23. For the segmentation network, the number of sampling points was 2048. We trained the network for up to 401 epochs, with a batch size of 12. For each network, we used the Adam optimizer with a learning rate of 10^{-3}.

4.4 Results

The receiver operating characteristic (ROC) curve and confusion matrix of each classification network are shown in Figure 6. It can be observed that all areas of the ROC curves are higher than 0.95, demonstrating that the trained classification networks are generalized. The sensitivities to the aneurysm class of the five networks were 73.63%, 81.08%, 79.49%, 86.11%, and 80.77%, respectively. This shows that we can precisely detect fragments with IA portions. By analyzing the confusion matrices, we observed that only a few fragments with aneurysms were misclassified because they had tiny aneurysms or contained only a small part of the aneurysm. However, a 100% sensitivity is not necessary for our classification network because the sampled fragments overlap, as shown in Figure 7. According to our sampling algorithm, the 80% sensitivity of the classifier does not mean that 1/5 of the aneurysms were already missed before the segmentation step. In this experiment, only 5 out of 114 IAs were missing. The real sensitivity to IAs is satisfactory, as shown in Table 2. However, some fragments without IA were not classified correctly because the original data contained significant noise and the fragments had a shape very similar to a small part of the full aneurysms. These misclassified cases were also sometimes difficult for segmentation networks. Therefore, they did not have a significant impact on the final segmentation results.

Table 2: The sensitives of aneurysm fragments and whole IAs (%).

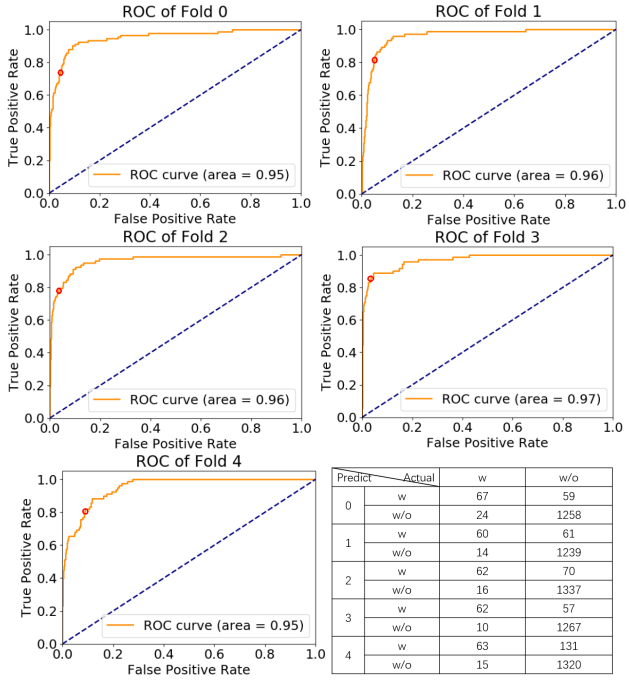
Fold	0	1	2	3	4
Fragments	73.63	81.08	79.49	86.11	80.77
Aneurysms	95.24	100.00	100.00	95.00	85.71

We added the classification step before segmentation to filter out the majority of fragments that did not contain aneurysms. This helped the segmentation network to avoid predicting false positive results on non-aneurysm regions, as well as, improving the balance between fragments with and without aneurysms, leading to better final segmentation accuracy. The benefit of the classification process is also shown in Section 4.5.2, in which we compare the proposed two-step pipeline and a segmentation-only pipeline.

Four examples of the final segmentation results are presented in Figure 8. In this figure, we show the entire 3D surface models and the enlarged important parts marked by black dotted boxes. The segmented aneurysms are colored in cyan, and other normal blood vessels are colored in red. We can see that our proposed pipeline obtained satisfactory segmentation results for various shapes and sizes of saccular aneurysms. We also found that unannotated potential aneurysms could also be segmented. However, a small amount of normal vessel ends were segmented as aneurysms because their shape were extremely similar to IAs. In addition, our networks predicted a suitable segmentation result for the fusiform aneurysm, even though they were trained only on saccular aneurysms. This demonstrates the excellent generalization ability of point-based deep learning models. Furthermore, our proposed pipeline obtained superb segmentation of multiple aneurysms in one case. A more detailed statistical analysis of our final segmentation results is provided in the comparison experiments 4.5.

4.5 Comparison experiments

4.5.1 3D U-Net. We first applied the original 3D U-Net to our data; however, the network cannot predict any segmentation result because the aneurysms were too small compared to the entire image.



Predict	Actual	w	w/o
0	w	67	59
	w/o	24	1258
1	w	60	61
	w/o	14	1239
2	w	62	70
	w/o	16	1337
3	w	62	57
	w/o	10	1267
4	w	63	131
	w/o	15	1320

Figure 6: ROC curves and confusion matrices of five trained classification networks.

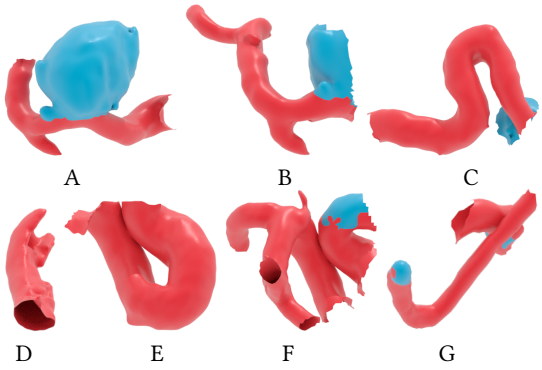
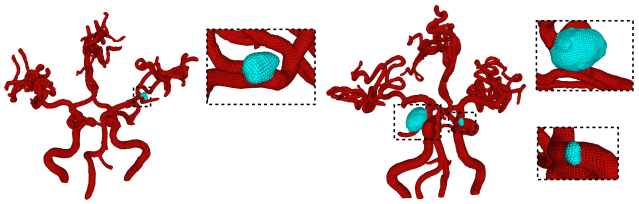


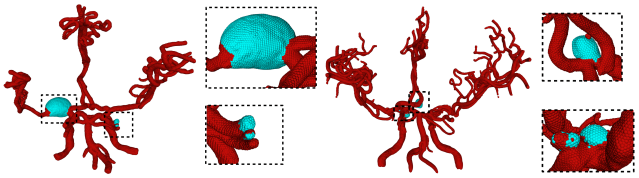
Figure 7: Fragment examples. Fragment A had a complete aneurysm. Fragments B and C partly overlap with A, but only include a part of the aneurysm. Fragments D, E, F, and G were without aneurysms, but were misclassified. The original data of D is noisy, and E, F, and G have a shape that is very similar to a part of the aneurysm.

This experiment demonstrates the difficulty of this segmentation task.

4.5.2 Segmentation only. To indicate the necessity of the two-step design, we performed an ablation study by removing the classification step from our proposed pipeline. That is, we fed all fragments to the pre-trained segmentation network to segment the aneurysm regions in the fragments. We compared the final results of this segmentation-only pipeline with those of the two-step pipeline on the entire artery surface models as shown in Table 3. The comparison results demonstrate that the classification step greatly reduces noise and improves the performance of the final segmentation result.



Left: Saccular aneurysms. The proposed pipeline obtained a perfect segmentation. Right: Saccular aneurysm. The aneurysm was segmented clearly without the impact of close blood vessels as shown in the top enlarged figure. A potential aneurysm was also predicted, which was not annotated by experts, as shown in the bottom enlarged figure.



Left: Fusiform aneurysms. The aneurysm was well segmented, as shown in the top enlarged figure. The ends of normal blood vessels were segmented incorrectly into aneurysms, as shown in the bottom figure. Right: Double saccular aneurysm; multiple aneurysms in one case. Two close aneurysms were annotated as one, and our segmentation did not achieve the same result as Yang et al. [25] because our training data included much more complex shapes.

Figure 8: Examples of final segmentation results (rendering in points); enlarged figures may be captured from a different viewpoint to show the aneurysm shape.

Table 3: Comparison of segmentation results between segmentation only and our two-step design on surface DSCs (%).

	Segmentation only		Two-steps	
	Mean	STD	Mean	STD
Overall	31.43	16.92	**74.74**	26.47
Fold 0	36.10	15.63	**76.73**	25.83
Fold 1	38.21	19.28	**80.18**	17.75
Fold 2	33.74	18.81	**80.66**	20.33
Fold 3	26.67	11.78	**73.78**	25.67
Fold 4	22.52	14.00	**62.54**	36.62

4.5.3 DeepMedic. We also applied the method described in [21] to our dataset for comparison. For preprocessing approaches A, B, C, and D were applied in their study. A has only been applied as a necessary step in DeepMedic, while B, C, and D, were used as additional masks for the skull-stripping of the TOF-MRA images. B generated the masks with a fixed threshold, C used a manual

Table 4: Comparison of segmentation results in DSCs (%).

	Ours (Surface-based)		DeepMedic S (Voxel-based)		DeepMedic B (Voxel-based)		3D U-Net (Voxel-based)	
	Mean	STD	Mean	STD	Mean	STD	Mean	STD
Overall	**71.79**	29.91	52.55	31.37	45.90	31.00	-	-
Fold 0	**73.10**	32.55	59.38	28.20	56.56	28.77	-	-
Fold 1	**75.72**	27.23	61.70	30.73	47.40	30.25	-	-
Fold 2	**73.81**	30.43	47.96	32.34	38.86	31.57	-	-
Fold 3	**72.37**	30.50	53.97	27.58	45.51	30.88	-	-
Fold 4	**64.17**	34.85	40.26	35.27	41.20	33.22	-	-

threshold for the skull-stripping of each sample, and D added N4 bias correction to the result of C. By analyzing the segmentation results, we found that skull-stripping could improve performance; however, there was not much difference between the results of B, C, and D. Therefore, we compared our method with B, which has the highest reproducibility. We used BET2 to obtain masks for skull-stripping using a fixed threshold of 0.2. The input of the TOF-MRA images was resized to 256×256 by down-sampling, according to the requirements of DeepMedic.

The DSC of the aneurysm parts was employed to evaluate the segmentation results. A comparison of the final segmentation results is shown in Figure 10 and Table 4. The performance of the voxel-based method was comparable to that reported in the original paper ([21]). Our surface-based method obtained much better segmentation results than the voxel-based method on most of the data. However, a few samples with tiny aneurysms were challenging both for the voxel-based method and for ours.



Figure 9: Left: a slice of the original MRA images. Middle: the corresponding ROI mask of skull-stripping generated by BET2. Right: the corresponding ROI surface mask generated by our surface model to provide the same input region for the DeepMedic model.

4.5.4 DeepMedic with surface mask (DeepMedic S). To directly compare performance between voxel-based and points-based networks, we generated artery region masks by converting our entire surface models into solid models and then mapping them back to the original MRA images, as shown in Figure 9. Thus, the voxel-based network obtained the same Region of Interest (ROI) as point-based models. We can see that the segmentation results were improved compared to the model trained with skull-stripping masks. However, the performance was still worse than that of our surface-based method. This comparative experiment shows that point-based networks can learn more accurate topological and geometric shape information compared to voxel-based models.

5 LIMITATION

Our current pipeline requires manual effort by medical experts to obtain surface models of intracranial artery networks. Thus, a possible criticism of our method is that this process severely limits its practical value. There are three reasons why we still believe that our method has significant practical value. First, neurosurgeons are presently already constructing surface models regularly in practice for preoperative examinations. Thus, we can assume that the surface model is already given in context. Second, the construction of the surface model is mostly performed through simple thresholding [9]. An expert manually sets a threshold, and voxels with intensities higher than the threshold are automatically extracted. In this process, the expert does not pay attention to the details of individual aneurysms. Aneurysms need to be carefully segmented manually using surface editing tools in current practice, and we expect automation of this process to be highly appreciated. Finally, we expect that, with the advances in deep learning methods, surface extraction will become largely or even fully automatic in the future. Consequently, the entire process may be fully automated, which has the potential to significantly impact the field.

Our experimental results show the baseline performance of the proposed framework. We believe that our results can be further improved significantly by adjusting hyper-parameters.

6 CONCLUSION

In this study, we proposed a new surface-based framework for the segmentation of intracranial aneurysms from TOF-MRA images. Our framework applied a two-step design, classification-segmentation, using state-of-the-art point-based deep learning networks. We also designed sampling and refinement methods for the IA segmentation task. The segmentation results show that our framework significantly outperforms the existing voxel-based method. Surface-based methods are as yet not prevalent in medical diagnosis and surgical planning. Our results show that surface-based methods can be a reliable alternative to popular voxel-based methods, and we hope this work may inspire further research efforts in this direction in other medical application domains.

ACKNOWLEDGMENTS

This research was supported by AMED under Grant Number JP18he1602001.

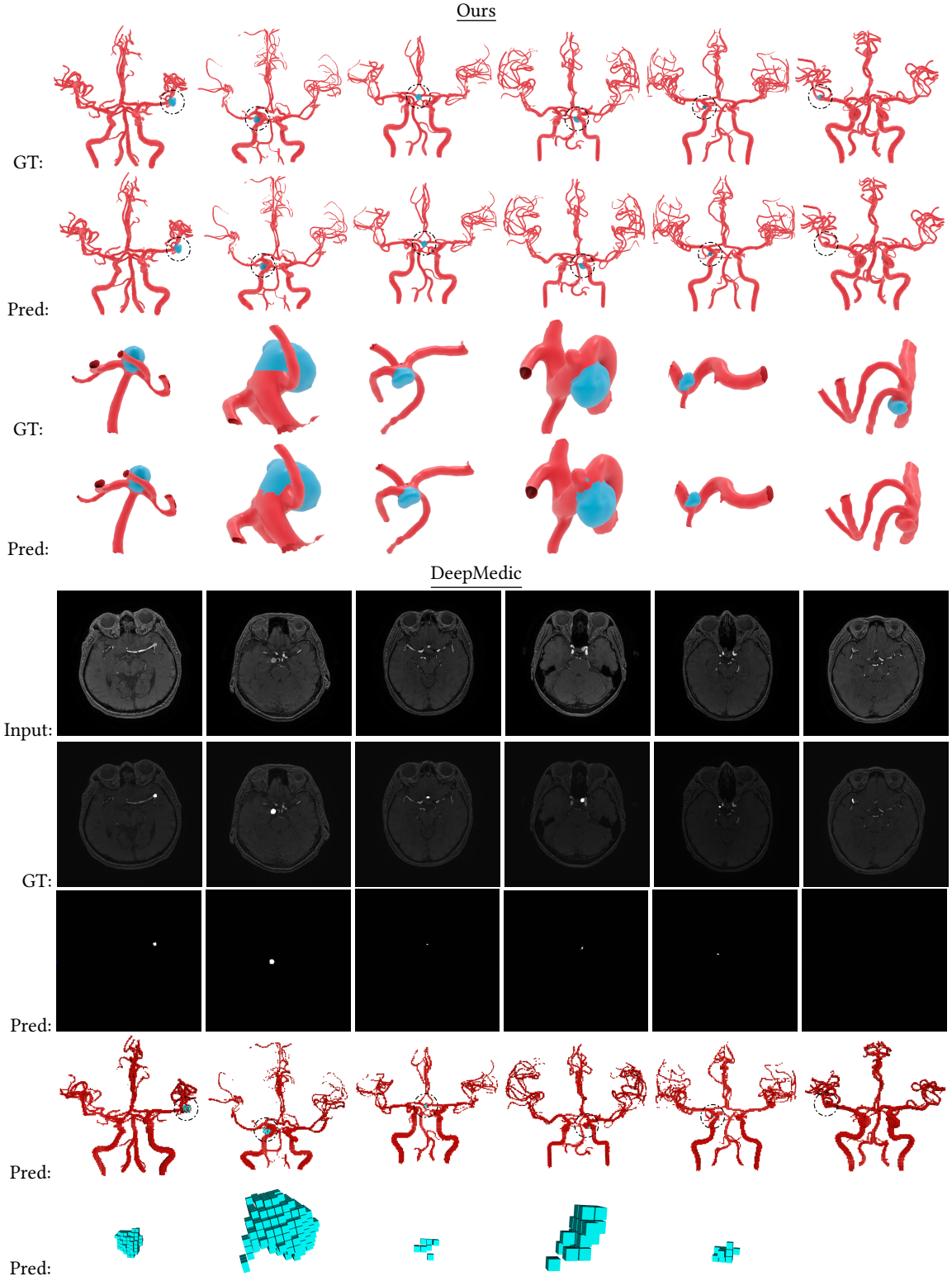


Figure 10: Comparison of segmentation results. Both our method and DeepMedic yielded high segmentation accuracy on the two examples (the leftmost two columns); our method yielded significantly better results than DeepMedic (the middle three columns); both our method and DeepMedic could not obtain the parts with IA (the rightmost column), as the fragment with the IA was filtered out by our classification network. We also show the predicted results of DeepMedic by volume (the last two rows).

REFERENCES

[1] Ali Alaraj, Cristian J Luciano, Daniel P Bailey, Abdussalam Elsenousi, Ben Z Roitberg, Antonio Bernardo, P Pat Banerjee, and Fady T Charbel. 2015. Virtual reality cerebral aneurysm clipping simulation with real-time haptic feedback. *Operative Neurosurgery* 11, 1 (2015), 52–58.

[2] Gavin Barill, Neil G Dickson, Ryan Schmidt, David IW Levin, and Alec Jacobson. 2018. Fast winding numbers for soups and clouds. *ACM Transactions on Graphics (TOG)* 37, 4 (2018), 1–12.

[3] Žiga Bizjak, Boštjan Likar, Franjo Pernuš, and Žiga Špiclin. 2020. Vascular surface segmentation for intracranial aneurysm isolation and quantification. *arXiv preprint arXiv:2005.14449* (2020).

[4] Sarada Prasad Dakua, Julien Abinahed, and Abdulla Al-Ansari. 2018. A PCA-based approach for brain aneurysm segmentation. *Multidimensional Systems and Signal Processing* 29, 1 (2018), 257–277.

[5] Rana Hanocka, Amir Hertz, Noa Fish, Raja Giryes, Shachar Fleishman, and Daniel Cohen-Or. 2019. MeshCNN: a network with an edge. *ACM Transactions on Graphics (TOG)* 38, 4 (2019), 1–12.

[6] UCAS Japan Investigators. 2012. The natural course of unruptured cerebral aneurysms in a Japanese cohort. *New England Journal of Medicine* 366, 26 (2012), 2474–2482.

[7] Tim Jerman, Aichi Chien, Franjo Pernuš, Boštjan Likar, and Žiga Špiclin. 2019. Automated Cutting Plane Positioning for Intracranial Aneurysm Quantification. *IEEE Transactions on Biomedical Engineering* 67, 2 (2019), 577–587.

[8] Konstantinos Kamnitsas, Christian Ledig, Virginia FJ Newcombe, Joanna P Simpson, Andrew D Kane, David K Menon, Daniel Rueckert, and Ben Glocker. 2017. Efficient multi-scale 3D CNN with fully connected CRF for accurate brain lesion segmentation. *Medical image analysis* 36 (2017), 61–78.

[9] Taichi Kin, Hirofumi Nakatomi, Masaaki Shojima, Minoru Tanaka, Kenji Ino, Harushi Mori, Akira Kunimatsu, Hiroshi Oyama, and Nobuhito Saito. 2012. A new strategic neurosurgical planning tool for brainstem cavernous malformations using interactive computer graphics with multimodal fusion images. *Journal of neurosurgery* 117, 1 (2012), 78–88.

[10] Philipp Krähenbühl and Vladlen Koltun. 2011. Efficient inference in fully connected crfs with gaussian edge potentials. In *Advances in neural information processing systems*. 109–117.

[11] Max WK Law and Albert CS Chung. 2007. Vessel and intracranial aneurysm segmentation using multi-range filters and local variances. In *International Conference on Medical Image Computing and Computer-Assisted Intervention*. Springer, 866–874.

[12] Max WK Law and Albert CS Chung. 2012. Segmentation of intracranial vessels and aneurysms in phase contrast magnetic resonance angiography using multirange filters and local variances. *IEEE Transactions on image processing* 22, 3 (2012), 845–859.

[13] Jiaxin Li, Ben M Chen, and Gim Hee Lee. 2018. So-net: Self-organizing network for point cloud analysis. In *Proceedings of the IEEE conference on computer vision and pattern recognition*. 9397–9406.

[14] Takahiro Nakao, Shouhei Hanaoka, Yukihiro Nomura, Issei Sato, Mitsutaka Nemoto, Soichiro Miki, Eriko Maeda, Takeharu Yoshikawa, Naoto Hayashi, and Osamu Abe. 2018. Deep neural network-based computer-assisted detection of cerebral aneurysms in MR angiography. *Journal of Magnetic Resonance Imaging* 47, 4 (2018), 948–953.

[15] Alireza Nikravanshalmani, Mojdeh Karamimohammdi, and Jamshid Dehmeshki. 2013. Segmentation and separation of cerebral aneurysms: A multi-phase approach. In *2013 8th International Symposium on Image and Signal Processing and Analysis (ISPA)*. IEEE, 505–510.

[16] Alireza Nikravanshalmani, Salah D Qanadli, Tim J Ellis, Matthew Crocker, Yousef Ebrahimdoost, Mojdeh Karamimohammadi, and Jamshid Dehmeshki. 2010. Three-dimensional semi-automatic segmentation of intracranial aneurysms in CTA. In *Proceedings of the 10th IEEE International Conference on Information Technology and Applications in Biomedicine*. IEEE, 1–4.

[17] Allison Park, Chris Chute, Pranav Rajpurkar, Joe Lou, Robyn L Ball, Katie Shpanskaya, Rashad Jabarkheel, Lily H Kim, Emily McKenna, Joe Tseng, et al. 2019. Deep Learning–Assisted Diagnosis of Cerebral Aneurysms Using the HeadXNet Model. *JAMA network open* 2, 6 (2019), e195600–e195600.

[18] Alexander R Podgorsak, Ryan A Rava, Mohammad Mahdi Shiraz Bhurwani, Anusha R Chandra, Jason M Davies, Adnan H Siddiqui, and Ciprian N Ionita. 2019. Automatic radiomic feature extraction using deep learning for angiographic parametric imaging of intracranial aneurysms. *Journal of neurointerventional surgery* (2019).

[19] Charles R Qi, Hao Su, Kaichun Mo, and Leonidas J Guibas. 2017. Pointnet: Deep learning on point sets for 3d classification and segmentation. In *Proceedings of the IEEE conference on computer vision and pattern recognition*. 652–660.

[20] Charles Ruizhongtai Qi, Li Yi, Hao Su, and Leonidas J Guibas. 2017. Pointnet++: Deep hierarchical feature learning on point sets in a metric space. In *Advances in neural information processing systems*. 5099–5108.

[21] T Sichtermann, A Faron, R Sijben, N Teichert, J Freiherr, and M Wiesmann. 2019. Deep Learning–Based Detection of Intracranial Aneurysms in 3D TOF-MRA. *American Journal of Neuroradiology* 40, 1 (2019), 25–32.

[22] Nisreen Sulayman, Moustafa Al-Mawaldi, and Qosai Kanafani. 2016. Semi-automatic detection and segmentation algorithm of saccular aneurysms in 2D cerebral DSA images. *The Egyptian Journal of Radiology and Nuclear Medicine* 47, 3 (2016), 859–865.

[23] Daiju Ueda, Akira Yamamoto, Masataka Nishimori, Taro Shimono, Satoshi Doishita, Akitoshi Shimazaki, Yutaka Katayama, Shinya Fukumoto, Antoine Choppin, Yuki Shimahara, et al. 2019. Deep learning for MR angiography: automated detection of cerebral aneurysms. *Radiology* 290, 1 (2019), 187–194.

[24] Yan Wang, Yue Zhang, Laurent Navarro, Omer Faruk Eker, Ricardo A Corredor Jerez, Yu Chen, Yuemin Zhu, and Guy Courbebaisse. 2016. Multilevel segmentation of intracranial aneurysms in CT angiography images. *Medical physics* 43, 4 (2016), 1777–1786.

[25] Xi Yang, Ding Xia, Taichi Kin, and Takeo Igarashi. 2020. IntrA: 3D Intracranial Aneurysm Dataset for Deep Learning. In *The IEEE Conference on Computer Vision and Pattern Recognition (CVPR)*. https://github.com/intra3d2019/IntrA

[26] Mingsong Zhou, Xingce Wang, Zhongke Wu, Jose M Pozo, and Alejandro F Frangi. 2019. Intracranial aneurysm detection from 3d vascular mesh models with ensemble deep learning. In *International Conference on Medical Image Computing and Computer-Assisted Intervention*. Springer, 243–252.